The Potential Role of Nitric Oxide in Substrate Switching in Eosinophil Peroxidase †

ARTICLE *in* BIOCHEMISTRY · FEBRUARY 2007

Impact Factor: 3.02 · DOI: 10.1021/bi061177u · Source: PubMed

4 AUTHORS, INCLUDING:

Semira Galijasevic
University of Sarajevo
22 PUBLICATIONS **285** CITATIONS

SEE PROFILE

The Potential Role of Nitric Oxide in Substrate Switching in Eosinophil Peroxidase†

Semira Galijasevic,‡ Gheorghe Proteasa,‡ Ibrahim Abdulhamid,# and Husam M. Abu-Soud*,‡,§

Departments of Obstetrics and Gynecology and Biochemistry and Molecular Biology, The C.S. Mott Center for Human Growth and Development and Department of Pediatrics, Children's Hospital of Michigan, Wayne State University School of Medicine, Detroit, Michigan 48201

Received June 13, 2006; Revised Manuscript Received September 15, 2006

ABSTRACT: Eosinophil recruitment and enhanced nitric oxide (NO) production are characteristic features of asthma and other airway diseases. Eosinophil peroxidase (EPO), a highly cationic hemoprotein secreted by activation of eosinophils, is believed to play a central role in host defense against invading pathogens. The enzyme uses hydrogen peroxide (H_2O_2) and bromide (Br^-), a preferred cosubstrate of EPO, to generate the cytotoxic oxidant hypobromous acid. The aim of this work was to determine whether NO can compete with plasma levels of Br^- and steer the enzyme reaction from a $2e^-$ oxidation to a $1e^-$ oxidation pathway. Rapid kinetic measurements were utilized to measure the rate of EPO compounds I and II formation, duration, and decay at 412 and 432 nm, respectively, at 10 °C. An EPO-Fe(III) solution supplemented with increasing Br^- concentrations was rapidly mixed with fixed amounts of H_2O_2 in the absence and in the presence of increasing NO concentrations. In the absence of NO, EPO-Fe(III) primarily converted to compound I and, upon H_2O_2 exhaustion, it decayed rapidly to the ferric form. NO caused a significant increase in the accumulation of EPO compound II, along with a proportional increase in its rate of formation and duration as determined by the time elapsed during catalysis. The time courses for these events have been incorporated into a comprehensive kinetic model. Computer simulations carried out supported the involvement of a conformational intermediate in the EPO compound II complex decay. Collectively, our results demonstrated that NO displays the potential capacity to promote substrate switching by modulating substrate selectivity of EPO.

Eosinophils are white blood cells that play a fundamental role in host defense mechanisms and in resisting infection caused by parasites in the body (*1*−*5*). They also play a role in tissue surveillance and allergic response mechanisms (*6*−*8*). The eosinophils make up about 2.3% of the total white blood cells and are found as granules in airways, sputum, and bronchoaveolar lavage fluid as well as the asthmatic bronchial tissue (*1*). Eosinophil peroxidase (EPO)[1] is secreted from the granules during phagocyte activation (*1*, *6*, *7*, *9*−*17*). EPO is a monomeric hemoprotein comprised of light and heavy chains with molecular masses of 50 and 15.5 kDa, respectively (*18*). EPO and related mammalian peroxidases [myeloperoxidase (MPO) and lactoperoxidase (LPO)] utilize H_2O_2 as the electron acceptor in the catalysis of oxidative reactions, which have a role in generating inflammatory injury and cardiovascular diseases (*6*, *10*, *12*−*14*, *19*). The enzyme catalyzes the formation of antimicrobial species, cytotoxic hypobromous acid, by the oxidation of bromide (Br^-) as a favored substrate (*18*, *20*, *21*) and functions as a catalytic sink for nitric oxide (NO) modulating its bioavailability (*22*−*26*). NO influences the type of oxidation reactions available to the hemoprotein by modulating the distribution of the intermediate forms during steady-state in EPO catalysis (*22*).

Bromide is one of the most abundant inorganic anions in human plasma and tissues (*27*). It is essentially present in every biological fluid, at a concentration of 20−150 μM (*28*). Animal studies have indicated that bromide deficiency is associated with a decrease in red-blood cell count, depressed growth, decrease in fertility and life expectancy, increase in milk fat, and increase in the number of spontaneous abortions (*28*−*33*). The most striking effects of high levels of Br^- intake on the endocrine system in animal models were found on the thyroid gland and the gonads, which typically lead to marked hypothyroidism (*32*). Higher Br^- levels may also cause a disturbance in the physiological function of the stomach, a decrease in iodide accumulation in the thyroid, and a rise in iodide excretion by kidneys (*32*). EPO is the only human enzyme known to selectively generate reactive brominating species under physiological concentration of halides (*34*−*36*). Brominated products can serve as markers to identify sites of EPO-mediated oxidative damage (*6*, *37*).

NO plays important roles in airway functions. NO, a gaseous signaling molecule, is generated by a family of enzymes called nitric oxide synthases (NOSs) (*38*). Inducible nitric oxide synthase (iNOS) is associated with most diseases involving overproduction of NO (*38*, *39*). The enzyme is

† This work was supported by a grant from the National Institutes of Health (HL066367, H.M.A.-S.) and by an award from the American Heart Association (S.G.).

* To whom correspondence should be addressed. Husam Abu-Soud, Ph.D., Wayne State University School of Medicine, Department of Obstetrics and Gynecology, The C.S. Mott Center for Human Growth and Development, 275 E. Hancock Detroit, Michigan 48201. Tel. 313 577-6178. Fax. 313 577-8554. E-mail: habusoud@med.wayne.edu.

‡ Department of Obstetrics and Gynecology.

§ Department of Biochemistry and Molecular Biology.

Department of Pediatrics.

[1] Abbreviations: Br^-, bromide; Cl^-, chloride; EPO, eosinophil peroxidase; H_2O_2, hydrogen peroxide; I^-, iodide; MPO, myeloperoxidase; NO, nitric oxide (nitrogen monoxide); SCN^-, thiocyanate.

10.1021/bi061177u CCC: $37.00
Published on Web 12/16/2006

usually able to operate at only a fraction of its maximum activity due to its regulation through equilibrium binding of soluble NO to ferric heme iron (*25*, *40*, *41*). Destabilizing the iNOS−nitrosyl complex, however, can restore the iNOS productivity (*25*). Indeed, NO scavengers such as MPO−H_2O_2 system, oxyhemoglobin, and superoxide-generating system can potentially enhance the catalytic activity of iNOS by preventing the formation of iNOS−nirosyl complex (*25*, *40*, *41*). We recently demonstrated that NO modulates the catalytic activity of EPO in a biphasic manner (*22*). In the active cycle, mammalian peroxidases catalyzed the oxidation of H_2O_2 generating a ferryl π cation radical (Fe(IV)═$O^{\bullet+\pi}$) intermediate known as compound I (*9*, *10*, *34*, *42*). This compound possesses the ability to oxidize halides and pseudo halides through a $2e^-$ transition generating the ground state (Fe(III)) and the corresponding hypohalous acids (*9*, *10*, *34*, *42*). Peroxidases can conversely oxidize NO by two successive $1e^-$ transitions, generating nitrosonium cation (NO^+) and the peroxidase intermediate compound II (Fe(IV)═O) and EPO-Fe(III) (*22*). The influence of a low NO concentration on compound II formation and decay rates indicates that NO serves as a physiological substrate for mammalian peroxidases (*22*). In this report, we examined how NO influences the catalytic activity of EPO during steady-state catalysis. Our rapid kinetic measurements indicate that NO displays the potential capacity to compete with Br^-, the preferred substrate of the enzyme, and steers the reaction from a $2e^-$ to a $1e^-$ oxidation pathway.

MATERIALS AND METHODS

Materials. NO gas was purchased from Matheson Tri-Gas Products, Inc. (Montgomeryville, PA) and used without further purification. For each experiment, a fresh saturated stock of NO was prepared under anaerobic conditions. The extent of nitrite/nitrate (NO_2^-/NO_3^-) build-up in NO preparations over the time course used for the present studies was <1−1.5% (per mol NO), as determined by anion exchange HPLC under anaerobic conditions (*43*). All other reagents and materials were of the highest purity grades available and obtained from Sigma Chemical Co. (St. Louis, MO) or the indicated source.

General Procedures. Porcine EPO was isolated using a modification of the method of Jorg, as described using guaiacol oxidation as the assay (*44*). Purity of isolated EPO was established by demonstrating a Reinheitzal (RZ) value of >0.9 (A_{412}/A_{280}), SDS−PAGE analysis with Coomassie Blue staining and gel tetramethylbenzidine peroxidase staining to confirm no contaminating MPO activity (*45*). An extinction coefficient of 112 000 M^{-1} cm^{-1}/heme of EPO was used to determine the final EPO concentration used in each experiment (*46*, *47*).

Optical Spectroscopy and Rapid Kinetic Measurements. Optical spectra were recorded on a Cary 100 Bio UV−visible spectrophotometer at 25 °C. Anaerobic spectra of EPO forms were recorded using septum-sealed quartz cuvettes that could attach through a quick-fit joint to a vacuum system. The peroxidase samples were made anaerobic by repeated cycles of evacuation and equilibrated with catalyst-deoxygenated N_2. Cuvettes were maintained under N_2 or NO atmosphere during spectral measurements. The kinetic measurements of EPO compound I and/or compound II formation and decay

Scheme 1: Comprehensive Kinetic Model for NO and Br^- Interactions with EPO

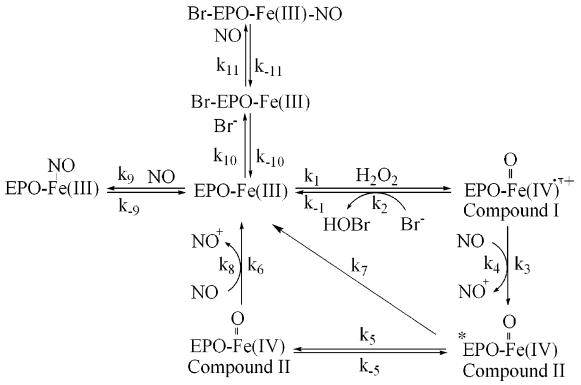

in the absence and presence of different NO and/or Br^- concentrations were performed using a dual syringe stopped-flow instrument obtained from Hi-Tech, Ltd. (model SF-61). Experiments were initially performed under conditions identical to those recently reported for EPO and MPO to facilitate comparisons (*22*−*26*). Measurements were carried out under an anaerobic atmosphere at 10 °C following rapid mixing of equal volumes of an H_2O_2-containing buffer solution and a peroxidase solution that contained different NO and/or Br^- concentrations. Reactions were monitored at both 412 and 432 nm. The time course of the absorbance change was fit to the following: simple linear equation, single-exponential, ($Y = 1 - e^{-kt}$), or double exponential ($Y = Ae^{-k_1t} + Be^{-k_2t}$) functions as indicated. Signal-to-noise ratios for all kinetic analyses were improved by averaging at least six to eight individual traces. In some experiments, the stopped-flow instrument was attached to a rapid scanning diode array device (Hi-Tech) designed to collect multiple numbers of complete spectrum (200−800 nm) at specific time ranges. The detector was automatically calibrated relative to a holmium oxide filter, as it has spectral peaks at 360.8, 418.5, 446.0, 453.4, 460.4, 536.4, and 637.5 nm, which were used by the software to correctly align pixel positions with wavelength. Rapid scanning experiments involve mixing solutions of peroxidase (1−2 μM) preincubated with 400 μM Br^- in the absence or in the presence of increasing (4−80 μM) NO concentrations with buffer solutions containing 40 μM H_2O_2, at 10 °C.

Solution Preparation. A fresh saturated stock of NO was prepared under anaerobic conditions. Anaerobic 0.2 M sodium phosphate buffer solutions, pH 7.0, containing various concentrations of NO were prepared by mixing different volumes of buffer saturated with NO gas at 21 °C with anaerobic buffer solution. A saturating concentration of NO at 21 °C is approximately 2 mM.

Model Simulations. The kinetic data collected from the stopped-flow was transferred to a Dell computer and subsequently processed with Reaction Kinetics Software (ChemSW; Fairfield, CA), using the comprehensive kinetic model that appears in Scheme 1. The rate constants used in the simulation process were either from experiments at 10 °C or were values from other experiments adjusted for temperature differences. The initial concentrations of Br^- and EPO that were used in the computer simulation were 400 and 1 μM, respectively.

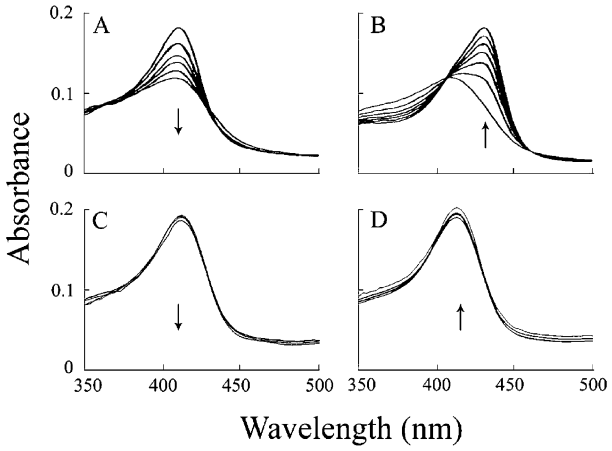

FIGURE 1: Spectral changes for the reaction of EPO-Fe(III) with H_2O_2 in the absence and the presence of Br^-. Panels A and B show EPO compound I formation and its conversion to compound II, respectively, when an anaerobic buffer solution (sodium phosphate 200 mM, pH 7.0) supplemented with 1.0 μM EPO-Fe(III) rapidly mixed with an equal volume of a buffer solution supplemented with 40 μM H_2O_2, using rapid scanning diode array instrument, at 10 °C. Panel A contains spectral collected at 0.001, 0.002, 0.003, 0.0045, 0.006, and 0.035 s after initiating the reaction, while panel B contains spectra collected at 0.5, 1, 3, 6.5, 10.5, and 20 after initiating the reaction. Panels C and D show spectral changes when the same reaction was repeated in the presence of 400 μM Br^- (final concentration). Panel C contains spectra collected at 0.01, 0.0032, 0.0073, and 0.015 s while panel D contains spectra collected at 0.02, 0.2, 5, and 20 s after initiating the reaction. Arrows indicate the direction of spectral change over time.

RESULTS

Effect of Increasing Br^- and NO Concentrations on EPO Intermediates Distribution During Steady-State Catalysis. The reaction between EPO-Fe(III) and H_2O_2 generates compound I, which was characterized by a significant decrease in the extinction coefficient of the Soret absorbance peak at 412 nm, as previously reported (Figure 1A) (*48*, *49*). The peroxidase intermediate formed within the first few milliseconds of initiating the reaction was unstable and rapidly converted within the following several seconds to a more stable peroxidase intermediate, compound II (E−Fe-(IV)═O) (*48*, *49*). EPO compound II displays a Soret absorbance peak centered at 432 nm and visible bands centered at 537 nm, typical of a six-coordinate complex (Figure 1B). This intermediate was relatively stable and decayed slowly to ground state in the next 500 s with a pseudo first-order rate constant of 0.005 s^{-1}.

We next utilized diode array spectrophotometry to probe the effect of Br^- on EPO intermediates formation, duration, and decay as they occur during steady-state catalysis. Investigations were carried out by rapid mixing of the enzyme solution (1.2 μM) supplemented with increasing Br^- concentrations against an equal volume of a buffer solution supplemented with 40 μM H_2O_2, at 10 °C. When a 1:1 ratio of H_2O_2 to Br^- was used, the majority of EPO-Fe(III) (80−90%) was converted to compound I and decayed immediately to the ground state upon H_2O_2 consumption. Increasing Br^- concentrations decreased EPO compound I accumulation, as judged by the attenuation in the amplitude of the Soret absorbance peak at 412 nm. Figure 1C,D shows the spectral changes that occur in the EPO Soret absorbance peak when the reaction was carried out in the presence of 400 μM Br^- (final concentration). When the Br^- concentration used was less than the H_2O_2 concentration (e.g., 10 and 20 μM), the majority of EPO-Fe(III) was converted to compound II upon H_2O_2 exhaustion.

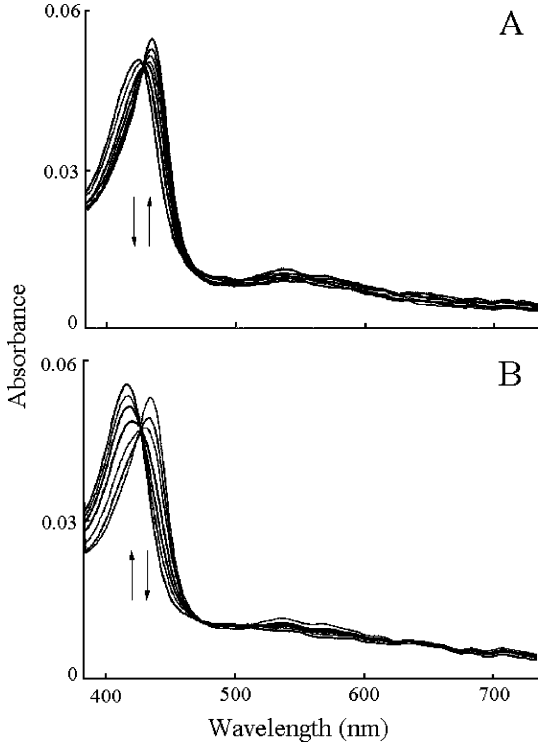

FIGURE 2: Spectral changes of Br^- metabolism by EPO-Fe(III) in the presence of NO during steady-state catalysis. Depicted is the absorbance change over time for the reaction that was initiated by rapidly mixing a buffer solution containing 40 μM H_2O_2 with an equal volume of a buffer solution containing 1.0 μM EPO-Fe(III), 400 μM Br^-, and 20 μM NO, using stopped-flow diode array methods at 10 °C. Panel A: spectra collected at 0.01, 0.015, 0.025, 0.04, 0.053, 0.08, and 0.5 s after initiating the reaction. Panel B: spectra collected at 0.6, 14, 17, 19, 22, 25, and 100 s after initiating the reaction. Arrows indicate the direction of spectral change over time.

To determine the influence of NO on the formation, duration, and decay of EPO intermediates distribution during steady-state catalysis, the same reactions were repeated in the presence of 400 μM Br^- and 20 μM NO. NO enhanced the accumulation of EPO compound II, as judged by the increased amplitude of the Soret absorbance peak at 432 nm, which went hand in hand with a proportional increase in the formation and decay rates of the complex. EPO compound II formed within 60 ms after mixing at 10 °C. Figure 2, Panel A illustrates spectral traces collected at 0.01, 0.015, 0.025, 0.04, 0.053, 0.08, and 0.5 s after initiating the reaction. This EPO intermediate was unstable and rapidly converted to ground state within 3 s. Figure 2B shows spectra collected at 0.6, 14, 17, 19, 22, 25, and 100 s after initiating the reaction. Spectral transitions between EPO compound II and the ground state revealed distinct isosbestic points (Figure 2B). The appearance of one set of isosbestic points suggests that only two components were present, in this case, EPO compound II and EPO-Fe(III). Therefore, sequential formation and decay of EPO compound II occurred at sufficiently different rates to allow each process to be studied by conventional (i.e., single mixing) stopped-flow methods.

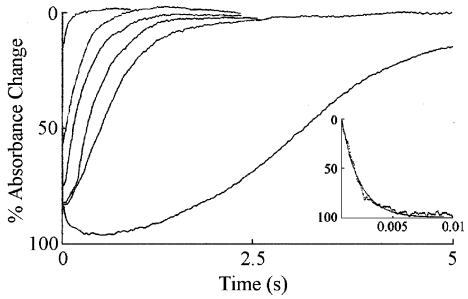

FIGURE 3: Spectral changes of Br^- metabolism by EPO-Fe(III) during steady-state catalysis at six different Br^- concentrations. Formation, duration, and decay of the steady-state catalysis of EPO-Fe(III) were monitored as a function of time at 412 nm. An aerobic solution containing 1.0 μM EPO-Fe(III) was preincubated with different concentrations of Br^- was rapidly mixed with an equal volume of sodium phosphate buffer (200 mM, pH 7.0) supplemented with 40 μM H_2O_2 at 10 °C. The initial concentration of Br^- in the mixtures is 20, 40, 100, 200, 400, 800, and 400 μM from bottom to top. The inset shows absorbance change from the third trace from the bottom within an initial time period. Trace contains line of best fit that was calculated using a single-exponential equation to describe absorbance change. The data are representative of at least three experiments each.

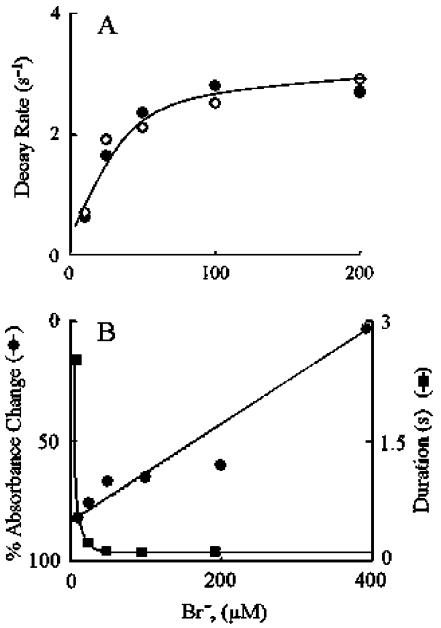

FIGURE 4: Rate of EPO-Fe(III) compound I decay, accumulation, and duration as a function of Br^- concentration. Panel A shows the relationship between Br^- concentration and the decay rate constant of EPO Compound I obtained at 412 nm (○) and at 432 nm (●). Panel B shows the relationship between Br^- concentration and the accumulation (●) and the duration (■) of EPO Compound I at 412 nm.

For a closer look at the reaction mechanism of the metabolism of Br^- by EPO, we next investigated the influence of Br^- on the kinetics of EPO compound I buildup, duration, and decay by following the decrease in absorbance at 412 nm using single wavelength stopped-flow methods (Figure 3). Experiments were carried out under aerobic conditions following rapid mixing of (40 μM) H_2O_2 and (1.0 μM) enzyme solution preincubated with various concentrations of Br^-, ranging from 20 to 800 μM. In the presence of 20 μM Br^-, the decrease in absorbance was biphasic with rate constants of 600 s^{-1} for the faster phase and 0.5 s^{-1} for the slower phase. Only the fast phase was observed when the Br^- concentration exceeded the H_2O_2 concentration

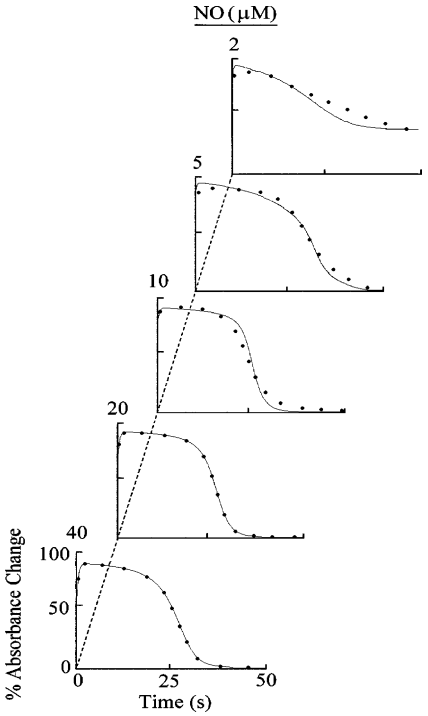

FIGURE 5: Effect of NO concentration on EPO-Fe(III) compound II formation, duration, and decay during steady-state metabolism of Br^-. Formation and decay of compound II of EPO-Fe(III) was monitored as a function of time by observing spectral changes at 432 nm (●). An anaerobic solution containing sodium phosphate buffer (200 mM, pH 7.0) supplemented with H_2O_2 (40 M) was rapidly mixed with an equal volume of buffer containing 1.0 μM of EPO-Fe(III), 200 μM Br^-, and differing concentrations of NO at 10 °C. The final concentration of NO in the mixtures is indicated in micromolar. The symbols represent portions of the experimental data, while the solid lines represent the simulated time courses using the rate constants that appear in the result section and the model in Scheme 1.

(Figure 3 inset). Two distinct phases in the decay of the steady state were also observed with apparent rate constants of 0.47 s^{-1} for the faster phase and 0.005 s^{-1} for the slower phase. In both the formation and the decay reactions, only the faster phases were observed upon increasing the Br^- concentration. As the concentration of Br^- present in the reaction mixture was increased, both the steady-state level and the buildup of the generated intermediate progressively decreased, while the decay rate increased in a linear and saturable manner (Figure 4).

Single wavelength stopped-flow spectroscopy was also utilized to investigate how NO interacts with the EPO and switches the reaction from a $2e^-$ to a $1e^-$ oxidation pathway during the metabolism of Br^-. Investigations were carried out by rapid mixing of EPO-Fe(III) solution preincubated with 200 μM Br^- in the presence of increasing concentrations of NO (e.g., 5, 10, 20, 40, and 80 μM) against 40 μM H_2O_2. In all cases, EPO compound II formation occurred without any indication of the buildup of compound I. Figure 5 shows actual stopped-flow traces for the build-up, duration, and decay of EPO compound II collected at 432 nm in the presence of increasing NO concentrations. In the presence of 5 μM, there was a fast buildup of EPO compound II, which remains at the same level for around 5 s. It decays through a biphasic reaction to the ferric form with apparent rate constants of 0.08 s^{-1} for the faster phase and 0.005 s^{-1} for the slower phase. At higher NO concentrations, only the

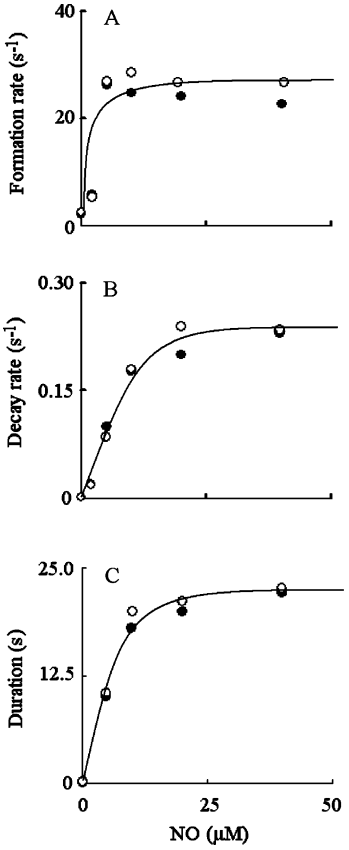

FIGURE 6: Rate of EPO-Fe(III) compound II formation, duration, and decay as a function of NO concentration. The observed rates of EPO-Fe(III) compound II formation (A), decay (B), and duration (C) [monitored at 432 (○) and 412 (●) nm] observed in Figure 5 were plotted as a function of NO concentration.

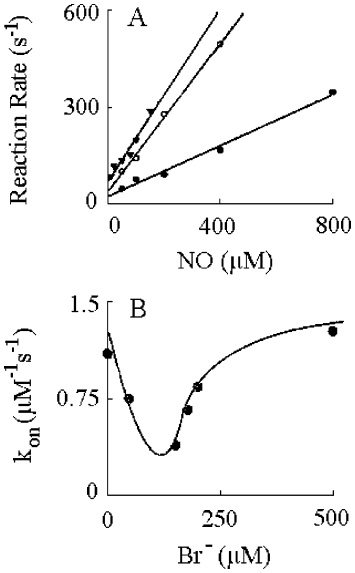

FIGURE 7: Br^- modulates NO binding to EPO heme iron. Plots of the observed rates of NO binding to EPO-Fe(III) as a function of NO and Br^- concentrations (A). An anaerobic solution containing 1.0 μM EPO-Fe(III) supplemented with 0 (▼), 150 (●), and 500 (○) μM Br^- was rapidly mixed with an equal volume of sodium phosphate buffer (200 mM at pH 7.0) supplemented with varying concentration of NO at 10 °C. Some of the lines were omitted from the panel for clarity. Biphasic effects were observed when the second-order combination rate constants (k_{on}) of NO binding calculated from the slope were plotted as a function of Br^- (B). The high concentration of the phosphate buffer is to keep the pH of the solution unaltered after the addition of NO.

faster phase was observed (Figure 5). Figure 6 shows the relationship between NO concentration and the rate of EPO compound II formation (panel A), duration of its formation (panel B), and the rate of complex decay (panel C). It was evident as NO concentration increased, the EPO compound II formation rate constant, complex duration, and decay rate progressively increased in linear and saturable manners. When the same reactions were monitored at 412 nm, the direction of absorbance change reversed and the signal amplitudes increased but otherwise proceeded with identical kinetics (Figure 6).

Effects of Br^- on NO Binding to EPO-Fe(III) Heme Iron. To assess the influence of Br^- on the catalytic activity of EPO, the rates of NO binding to the Fe(III) form of EPO were determined in the presence of increasing Br^- concentrations. Investigations were carried out under either a fixed amount of NO and varying concentrations of Br^-, or a fixed amount of Br^- and varying levels of NO. As shown in Figure 7A, the plots of the apparent rate constants for NO binding as a function of NO concentration were linear, consistent with a simple one-step mechanism. The positive intercepts confirm that NO binds to EPO-Fe(III) in a reversible process, as shown in eq 1. These kinetic parameters suggest that Br^- modulates the affinity of EPO-Fe(III) toward NO. The second-order combination rate constants (k_{on}) calculated from the slopes plotted as a function of Br^- concentration showed a bell-shaped relationship (Figure 7B). Interestingly, the observed minimum of the bell-shaped curve was centered at biologically relevant levels of Br^- (150 μM). Collectively, these results indicated that Br^- binds within the enzyme system and modulates the affinity of EPO-Fe(III) toward NO.

$$\text{Br-EPO-Fe(III)} + \text{NO} \underset{k_{off}}{\overset{k_{on}}{\leftrightarrow}} \text{Br-EPO-Fe(III)-NO} \quad (1)$$

Computer Simulation. All of the kinetic data collected from the stopped-flow studies were transferred to a Dell computer and, subsequently, analyzed with Reaction Kinetics program, using the comprehensive kinetic model that appears in Scheme 1. Numeric integration of the partial differential equations describing the reactions was used in the computer simulations. We were unable to simulate all the time courses illustrated in Figure 5 without incorporating a conformational step (*EPO-Fe(IV)═O ↔ EPO-Fe(IV)═O) into our proposed kinetic model (Scheme 1). This conformational intermediate limits the decay of EPO compound II to the ferric state. The rate constants for the formation of EPO compound I and its decay to the ground state (k_1, k_{-1}), the rate constant for the reaction of compound I with Br^- to generate the corresponding hypohalous acid (k_2), the rate constants for the formation of compound II and decay to the ground state in the presence and the absence of NO (k_3, k_4, k_6, k_7, and k_8), and the rate of EPO-Fe(III)-NO formation and its decay (k_9 and k_{-9}) have been previously reported (*22*, *48*, *49*, *50*). The rate constant for the reaction of NO with of EPO-Fe(III) in the presence of 200 μM Br^- (k_{11} and k_{-11}) have been taken from the current study. All these rate constants were temperature corrected and kept constant during the simulation.

The remaining microscopic rate constants that appear in this kinetic model (k_5, k_{-5}, k_{10}, and k_{-10}) were estimated by comparison of the experimental time courses for the ac-

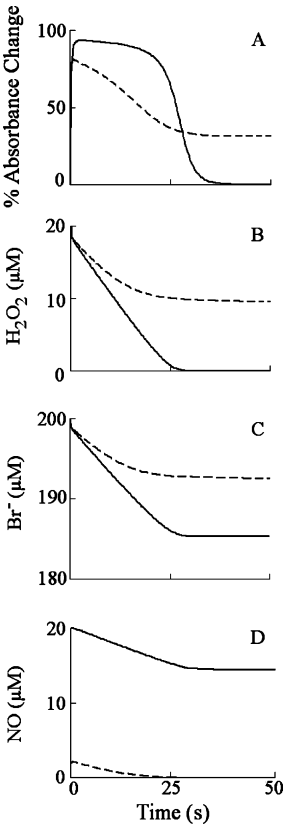

FIGURE 8: Computer simulation of the reactions depicted in Scheme 1. (A) Simulated time courses for the progression of the reaction of EPO-Fe(III) preincubated with Br^- when the reaction was monitored at 432 nm in the presence of 2 μM (- - -) and 20 μM (−) NO. Panels B, C, and D apply to H_2O_2, Br^-, and NO consumption for the same reactions, respectively.

cumulation of EPO compound II during steady-state catalysis with the calculated time courses derived by numerical integration of the appropriate differential equations with the simulation program. These rate constants were first estimated graphically based on the known related kinetic model of MPO (*26*). The final values were then adjusted by minimization of the difference between the experimental and simulated data until the simulated time courses matched the experimental data as closely as possible (Figure 5).

k_1 - The reaction between EPO-Fe(III) and hydrogen peroxide was given a rate constant of 7.0×10^6 s^{-1} M^{-1} based on experimental value (*48*, *49*).

k_{-1} - Reverse rate constant value for the decay of compound I back to EPO-Fe(III) was 5.0 s^{-1} (*48*, *49*).

k_2 - The rate constant for the $2e^-$ reduction of Br^- by EPO compound I was assigned a rate constant of 5.5×10^6 M^{-1} s^{-1} (*48*, *49*).

k_3 - The rate of conversion of compound I to compound II was given a rate constant of 8.00×10^2 M^{-1} s^{-1}, as previously reported (*48*, *49*). A great variety of electron donors mediate this transformation including H_2O_2 (*51*, *52*).

k_4 - The conversion of compound I to compound II in the presence of NO was given a rate constant of 5.60×10^4 M^{-1} s^{-1} (*22*).

k_5 - The experimental data showed a conformational change of compound II and was given a rate constant of 0.46 s^{-1}.

k_{-5} - The reverse rate for the conformational change reaction was assigned a value of 0.2 s^{-1}.

k_6 - Decay of compound II to EPO-Fe(III) was given a rate constant of 0.005 s^{-1} (*22*).

k_7 - Decay of compound II* to EPO-Fe(III) was given a rate constant of 0.01 s^{-1} (*22*).

k_8 - The conversion of compound II to EPO-Fe(III) in the presence of NO was given a rate constant of 4.0×10^5 M^{-1} s^{-1} (*22*).

k_9 - Formation of EPO-Fe(III)-NO complex was given a rate constant of 1.39×10^2 M^{-1} s^{-1} as previously experimentally determined (*50*).

k_{-9} - Dissociation rate of EPO-Fe(III)-NO complex was assigned an experimental value of 2.0 s^{-1} (*50*).

k_{10} - EPO-Fe(III) reaction with Br^- present in excess in solution was given a rate constant of 2.9×10^5 M^{-1} s^{-1}. In this case, we assume that Br^- behaves as a substrate.

k_{-10} - Dissociation of free Br^- from the formed Br-EPO-Fe(III) was assumed to have a rate constant of 85 s^{-1}.

k_{11} - Experimentally determined value of 4.08×10^5 M^{-1} s^{-1} for the formation reaction between Br-EPO-Fe(III) complex and NO was used in computer simulation (*50*).

k_{-11} - Dissociation of NO from Br-EPO-Fe(III)-NO complex was given a rate constant of 6.0 s^{-1} (*50*).

Figure 8A shows the simulated time courses of EPO compound II at two different NO concentrations, 2 and 20 μM. The majority of the enzyme converted to compound II during the initial phase of the reaction and remained at the same level through the progress of the reaction, until all the H_2O_2 or the NO was depleted. Consumption of Br^- and NO were linear according to the model and ceased when H_2O_2 or NO was completely consumed (Figure 8B−D). The kinetic simulation also revealed that the amount of Br^- consumed by EPO-Fe(III) was significantly increased upon increasing NO concentration (Figure 8C).

DISCUSSION

Inflammation in the airways is typically associated with enhanced levels of EPO, MPO, and LPO, as well as increased concentrations of H_2O_2, a natural substrate of these three enzymes (*53*−*55*). The potential capacity of the peroxidase−H_2O_2 systems in consuming NO and the enzymes involvement in the endogenous formation of nitrating oxidants and halogenated tyrosine derivatives directly implicate the participation of peroxidase-dependent pathways in airway diseases and infection (*10*, *53*−*55*). NO overproduction is thought to play an important role in airway inflammatory diseases (*53*−*56*). Upregulation of inducible NO synthase gene expression and upregulation of its catalytic activity by preventing the NO feedback inhibition by peroxidase-H_2O_2 systems are thought to be important factors in this regard (*25*, *53*, *56*). Understanding the consequences of NO enhancement on mammalian peroxidases viability and identifying the conditions in which NO regulation contributes to substrate switching (steering the reaction from a $2e^-$ to $1e^-$ oxidation pathway) in mammalian peroxidases remains a topic of considerable interest and high potential importance.

Our current results clearly demonstrate that EPO is more vulnerable to NO-mediated substrate switching than MPO (*23*, *24*, *26*) as judged by the significant increase in EPO-Fe(III) absorbance at 432 nm, a hallmark of the EPO

compound II accumulation, during steady-state metabolism of Br^-. We have recently demonstrated that the order of addition (the enzyme and H_2O_2 mixed first and halide second, or the enzyme and halide mixed first and H_2O_2 second) plays an important role in the kinetic mechanism of mammalian peroxidases (*26*, *57*). This is due to the capacity of halides and pseudo halides to bind to the enzymes and function as a substrate or as an inhibitor (*33*, *58*−*60*, *61*). We have also demonstrated that EPO-Fe(III) is converted immediately to a stable EPO compound II without any sign of compound I accumulation when the enzyme is preincubated with SCN^- prior to initiating peroxidation (*57*). A working kinetic model incorporating our previous and current findings combined with EPO classic cycle is shown in Scheme 1. In the classic cycle, EPO-Fe(III) requires H_2O_2 to generate compound I (*9*, *10*, *34*, *42*, *48*, *49*). Compound I reacts with Br^- with an apparent second-order rate constant of 1.9×10^7 M^{-1} s^{-1} to produce the corresponding hypohalous acid (*48*, *49*). The direct reaction between compound I and Br^- prevents, to a large extent, the potential alteration in the heme pocket that occurs when the enzyme is incubated first with Br^- (*48*, *49*). Br^- deficiency allows subsequent conversion of EPO compound I to a more stable intermediate compound II, which in turn decays slowly to EPO-Fe(III).

Br^- displays a variable effect on the formation, duration, and decay of EPO compounds I and II, suggesting a multifunctional role for Br^- before and during steady-state catalysis. EPO was far from saturated in the presence of plasma levels of Br^- and at equilibrium; EPO-Fe(III) was present as free and bromide-bound forms. In the presence of low levels of Br^-, EPO compound I formation was biphasic. The rate constant of the faster phase was identical to the value observed for the rate constant of EPO compound I formation (*48*, *49*). The slower phase was attributed to the reaction of H_2O_2 with Br-bond EPO-Fe(III), similar to that previously reported when EPO-Fe(III) was first preincubated with SCN^- (*57*). Under these circumstances both the formation rate constants are faster than the rate of the $2e^-$ oxidation of Br^-, therefore, both were observable. In the presence of higher levels of Br^-, only the fast formation rate was observed implying that only the fast phase exceeded the rate of the $2e^-$ oxidation of Br^-. It appears that as the Br^- concentration increases, compound I is converted rapidly and more efficiently to EPO-Fe(III). This behavior is illustrated by the significant alteration in the intermediate distributions during steady-state catalysis, as reflected by the decrease in the amplitude of compound I formation observed in a Br^--dependent manner.

NO influences the time of the reaction (duration of the 432 nm signal), and the decay rate during Br^- metabolism. Again, as the NO concentration increases, compound I is converted rapidly and more efficiently to ground state through the accumulation of compound II. This mechanistic feature suggests that under physiological conditions where the presence of both Br^- and NO during EPO compound II catalysis is anticipated, NO plays a different role in each step of EPO catalysis. In the presence of biologically relevant levels of NO ($\leq$2.5 μM) and Br^- (100 μM), NO predominantly serves as a one e^- reductant for EPO compounds I and II, as reflected by the enhancement of EPO compound II accumulation and accelerated rates of complex formation and decay. The presumed intermediate formed, nitrosonium cation (NO^+) is remarkably unstable and rapidly hydrolyzed in aqueous solutions yielding nitrite (NO_2^-). Formation of NO_2^-, a substrate for EPO (*22*), at or near the heme moiety might also contribute to the increased overall transit time through the peroxidase cycle observed in the presence of NO. It would also serve to convert a relatively innocuous free radical species, NO, into a more noxious one, nitrogen dioxide (NO_2), which subsequently promotes lipid peroxidation, protein oxidation, and nitration (*34*, *36*, *42*, *62*). However, under our current experimental conditions the impact of NO_2^- deriving from NO or NO^+ on the observed kinetics was minimal, since high concentrations of nitrite is required to promote the loss of H_2O_2 (*63*).

In contrast, at higher levels of NO (i.e., when NO levels are higher than the K_{diss} for Fe(III)-NO), the majority of the enzyme is present in the NO-bound forms, Br-EPO-Fe(III)-NO and EPO-Fe(III)-NO complexes. Therefore, the dissociation rates of NO from the two complexes and the cleavage of Br^- from the Br-EPO-Fe(III) also account for the differences in the observed plots of NO concentration vs rate of compound II formation for the enzyme (Scheme 1). Thus, the rate-limiting step during steady-state catalysis shifts from reduction of compound II to dissociation of the NO from Fe(III)-NO complex and/or to the dissociation of Br^- from Br−Fe(III) complexes during steady-state catalysis (Scheme 1). Since the initial concentration of Br^- is kept constant at all NO concentrations used, the plot plateaus at a rate comparable to the dissociation rate constant for the respective Fe(III)-NO complexes. The relatively high dissociation rate of the EPO-Fe(III)-NO complex limits the amount of active peroxidase available during steady-state catalysis. Because EPO compound I formation rates are slower than the $2e^-$ oxidation of Br^- (*48*, *49*), compound I accumulation cannot be detected during steady-state catalysis. Thus, the observed absorbance changes during Br^- metabolism should reflect the alteration in the second slower intermediate, which is under these circumstances EPO compound II accumulation, duration, and decay.

The ability of Br^- to modulate the EPO heme pocket microenvironment is directly mirrored by the modulation of NO binding to the enzyme heme moiety. Indeed, the plot of the second-order combination rate constant (k_{on}) of NO binding to EPO-Fe(III) as a function of Br^- concentration displayed a bell-shaped relationship, with the trough centered at the plasma levels of Br^- (*28*). A similar behavior was also observed for MPO when the second-order combination rate constant of NO binding to MPO−Fe(III) was plotted as a function of Cl^-, I^-, Br^-, and SCN^- (*64*). MPO X-ray structure is presently available (*58*−*60*). Although these studies have suggested that halide binds as a substrate or as an inhibitor to the enzyme, they do not exclude the possibility for the existence of two separate halide-binding sites. Earlier studies by several groups have concluded that there are two separate sites on MPO for the binding of halides (*61*, *65*−*67*). Our recent rapid kinetic measurements are consistent with two halide binding sites for MPO that could be populated by two chloride atoms or by one chloride and the other by Br^-, I^-, or SCN^- (*64*). On the basis of our current kinetic studies and a theoretical EPO three-dimensional model built on the scaffold of the LPO X-ray structure (*68*, *69*), we speculate that Br^- binds at two different binding sites on EPO and both have distinct effects on the EPO heme

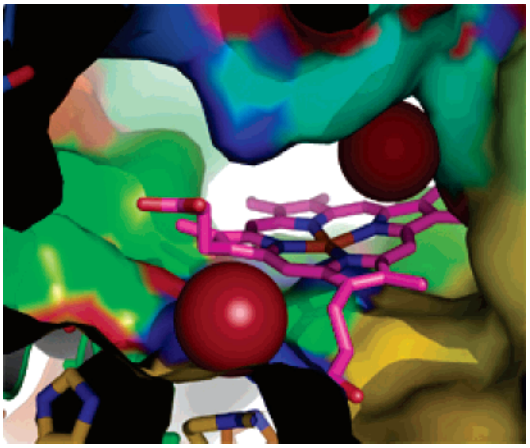

FIGURE 9: Theoretical three-dimensional model for EPO built on the scaffold of the LPO X-ray structure derived from Protein Data Bank structure 2GJ1 in which we introduced two Br^- atoms corresponding to the heme binding sites described in the paper. The figure was produced using coordinates from the protein data file with the pdb visualization program PyMOL (DeLano Laboratories).

iron microenvironment (Figure 9). The first Br^- binding site is represented by the triad of amino acids Arg337NH1, Leu384CD1, and Glu380OE1/OE2, while the second binding site for Br^- is putatively represented by Arg562NH2/NE, Arg471NH2, and His566NE2 which form the binding pocket. Consistent with this hypothesis, previous investigations of the 3D structures of a number of peroxidases (CCP, AP, LiP, and MnP) have shown the existence of two binding sites within the heme pocket microenvironment (*70*−*76*). On the basis of our kinetic measurements and the structural similarity of human EPO to other peroxidases, including LPO, MPO, CCP, AP, LiP, and, MnP, we conclude that EPO utilizes a dual heme pocket binding site configuration (*70*−*76*).

This behavior may be physiologically significant because the initial decrease in the second-order rate constant of NO combination (k_{on}) occurs within the range where Br^- binds to the distal cavity located in EPO compound I and allows the direct contact with the oxyferryl oxygen. Under these circumstances, compound I appears to act favorably in triggering electron transfer to the heme with subsequent conversion to hypobromous acid as a final reaction product (*58*−*60*). Therefore, the plasma level of Br^- (60 μM) is crucial in saturating the substrate site of the enzyme as judged by the inflection point in the bell-shaped curve. The plasma level of Br^- may consequently govern the catalytic reaction of EPO-Fe(III), both in vivo and in vitro. Changes in the heme pocket geometry upon ligand binding have been described for cytochrome C peroxidase and other related hemoproteins (*77*−*79*).

Our kinetic simulations have indicated the involvement of a compound II conformational intermediate that limits the EPO compound II decay rate to the ferric form (Scheme 1). This conformational intermediate is slow enough to kinetically be the rate-limiting step in the decay process in the presence of NO. It may take part in promoting the increase in the duration and in the amplitude of EPO compound II. Computer simulations also indicated that the build-up of compound II that is occurring in the first milliseconds of initiating the reaction was accompanied by a significant decrease in the rate of H_2O_2 reduction, as judged by a deflection in the rate of H_2O_2 consumption to a slower rate (Figure 8). The first phase of the reaction can be attributed to H_2O_2 oxidation of EPO-Fe(III), which precedes the formation of compound I. The subsequent decrease in the rate of H_2O_2 consumption can be attributed to the formation and accumulation of EPO compound II, the rate-limiting step in the peroxidase cycle. NO consumption continued linearly until all H_2O_2 was depleted (Figure 8). After H_2O_2 or NO was exhausted, the compound II signal decayed over a 3 s period. The amount of Br^- consumed by EPO-Fe(III) significantly increased upon increasing NO concentration (Figure 8). Thus, our kinetic data suggests that the build-up of compound II during steady-sate catalysis is a reaction driven by NO.

Collectively, preincubation of Br^- with EPO-Fe(III) significantly affects its catalytic site, subsequently altering heme iron reactivity, affecting the affinity toward ligand and substrate binding, and disturbing the intermediates distribution in a distinct manner, which can ultimately affect substrate selectivity and specificity. NO presence may play a potential role in promoting substrate switching during Br^- metabolism. Our current results suggest an important application in biological systems. Airway inflammatory processes, including asthma or airway infections, are associated with enhanced production of NO and high levels of EPO and related hemoprotein (MPO and LPO). High levels of NO are clearly important in antimicrobial host defense (*56*, *80*, *81*), but chronic NO overproduction is implicated in the pathophysiology of the airway inflammation and injury in asthma (*82*, *83*).

The airway environmental milieu, in conditions of airway infection or asthma, provide the ideal conditions for NO to compete with halides or pseudo halides and switch the mammalian peroxidase reactions from a $2e^-$ to a $1e^-$ oxidation pathway. This process would drive the peroxidase-H_2O_2 system to generate reactive oxygen and reactive nitrogen species, as well as to catalyze the H_2O_2-dependent peroxidation of halides and pseudo halides to produce hypohalous acids. This would be of benefit during times of infection by broadening the scope of host defense armamentarium but create increased toxicity in the chronic inflammation of asthma.

REFERENCES

1. Klebanoff, S. J., Locksley, R. M., Jong, E., and Rosen, H. (1983) Oxidative response of phagocytes to parasite invasion, *Ciba Found. Symp. 99*, 92−112.
2. Abraham, D., Leon, O., Schnyder-Candrian, S., Wang, C. C., Galioto, A. M., Kerepesi, L. A., Lee, J. J., and Lustigman, S. (2004) Immunoglobulin E and eosinophil-dependent protective immunity to larval *Onchocerca volvulus* in mice immunized with irradiated larvae, *Infect. Immun. 72*, 810−817.
3. Ackerman, S. J., Gleich, G. J., Loegering, D. A., Richardson, B. A., and Butterworth, A. E. (1985) Comparative toxicity of purified human eosinophil granule cationic proteins for schistosomula of Schistosoma mansoni, *Am. J. Trop. Med. Hyg. 34*, 735−745.
4. Betts, C. J., and Else, K. J. (1999) Mast cells, eosinophils and antibody-mediated cellular cytotoxicity are not critical in resistance to Trichuris muris, *Parasite Immunol. 21*, 45−52.
5. Chandrashekar, R., Rao, U. R., Parab, P. B., and Subrahmanyam. D. (1986) Brugia malayi: rat cell interactions with infective larvae mediated by complement, *Exp. Parasitol.* 62, 362−369.
6. Gleich, G. J., Ottesen, E. A., Leiferman, K. M., and Ackerman, S. J. (1989) Eosinophils and human disease, *Int. Arch. Allergy Appl. Immunol. 88*, 59−62.

7. Rothenberg, M. E. (1998) Eosinophilia, *N. Engl. J. Med. 338*, 1592−1600.
8. Holt, P. G., Macaubas, C., Stumbles, P. A., and Sly, P. D. (1999) The role of allergy in the development of asthma, *Nature 402*, B12−B17.
9. Weiss, S. J., Test, S. T., Eckmann, C. M., Ross, D., and Regiania, S. (1986) Brominating oxidants generated by human eosinophils, *Science 234*, 200−203.
10. Mayeno, A. N., Curran, A. J., Roberts, R. L., and Foote, C. S. (1989) Eosinophils preferentially use bromide to generate halogenating agents, *J. Biol. Chem. 264*, 5660−5668.
11. Agosti, J. M., Altman, L. C., Ayars, G. H., Loegering, D. A., Gleich, G. J., and Klebanoff, S. J. (1987) The injurious effect of eosinophil peroxidase, hydrogen peroxide, and halides on pneumocytes in vitro, *J. Allergy Clin. Immunol. 79*, 496−504.
12. Jong, E. C., Henderson, W. R., and Klebanoff, S. J. (1980) Bactericidal activity of eosinophil peroxidase, *J. Immunol. 124*, 1378−1382.
13. Jong, E. C., Mahmoud, A. A., and Klebanoff, S. J. (1981) Peroxidase-mediated toxicity to schistosomula of Schistosoma mansoni, *J. Immunol. 126*, 468−471.
14. Slungaard, A., and Mahoney, J. R., Jr. (1991) Bromide-dependent toxicity of eosinophil peroxidase for endothelium and isolated working rat hearts: a model for eosinophilic endocarditis, *J. Exp. Med. 173*, 117−126.
15. Klebanoff, S. J., Agosti, J. M., Jorg, A., and Waltersdorph, A. M. (1989) Comparative toxicity of the horse eosinophil peroxidase-H_2O_2-halide system and granule basic proteins, *J. Immunol. 143*, 239−244.
16. Kazura, J. W., Fanning, M. M., Blumer, J. L., and Mahmoud, A. A. (1981) Role of cell-generated hydrogen peroxide in granulocyte-mediated killing of schistosomula of *Schistosoma mansoni* in vitro, *J. Clin. Invest. 67*, 93−102.
17. Samoszuk, M. K., Nguyen, V., Thomas, C., and Jacobson, D. (1994) Effects of sonicated eosinophils on the in vivo sensitivity of human lymphoma cells to glucose oxidase, *Cancer Res. 54*, 2650−2653.
18. Bolscher, B. G., Zoutberrg, G. R., Cuperus, R. A., and Wever, R. (1984) Vitamin C stimulates the chlorinating activity of human myeloperoxidase, *Biochim. Biophys. Acta 784*, 189−191.
19. Klebanoff, S. J., Waltersdorph, A. M., and Rosen, H. (1984) Antimicrobial activity of myeloperoxidase, *Methods Enzymol. 105*, 399−403.
20. Caulfield, J. P., Korman, G., Butterworth, A. E., Hogan, M., and David, J. R. (1980) Partial and complete detachment of neutrophils and eosinophils from schistosomula: evidence for the establishment of continuity between a fused and normal parasite membrane, *J. Cell Biol. 86*, 46−63.
21. Arlandson, M., Decker, T., Roongta, V. A., Bonilla, L., Mayo, K. H., MacPherson, J. C., Hazen, S. L., and Slungaard, A. (2001) Eosinophil peroxidase oxidation of thiocyanate. Characterization of major reaction products and a potential sulfhydryl-targeted cytotoxicity system, *J. Biol. Chem. 276*, 215−224.
22. Abu-Soud, H. M., Khassawneh, M. Y., Sohn, J. T., Murray, P., Haxhiu, M. A., and Hazen, S. L. (2001) Peroxidases inhibit nitric oxide (NO) dependent bronchodilation: development of a model describing NO-peroxidase interactions, *Biochemistry 40*, 11866−11875.
23. Abu-Soud, H. M., and Hazen, S. L. (2000) Nitric oxide is a physiological substrate for mammalian peroxidases, *J. Biol. Chem. 275*, 37524−37532.
24. Abu-Soud, H. M., and Hazen, S. L. (2000) Nitric oxide modulates the catalytic activity of myeloperoxidase, *J. Biol. Chem. 275*, 5425−5430.
25. Galijasevic, S., Saed, G. M., Diamond, M. P., and Abu-Soud, H. M. (2003) Myeloperoxidase up-regulates the catalytic activity of inducible nitric oxide synthase by preventing nitric oxide feedback inhibition, *Proc. Natl. Acad. Sci. U.S.A. 100*, 14766−14771.
26. Galijasevic, S., Saed, G. M., Hazen, S. L., and Abu-Soud, H. M. (2006) Myeloperoxidase metabolizes thiocyanate in a reaction driven by nitric oxide, *Biochemistry 45*, 1255−1262.
27. Teitz, N. W. (1999) Drugs: Therapeutic and Toxic, in *Teitz Textbook of Clinical Chemistry* (Burtis, C.A., and Ashwood, E.R., Eds.) p 1097, W.B. Saunders Co., Philadelphia.
28. Faulkner, D. J. (1998) Marine natural products, *Nat. Prod. Rep. 15*, 113−158.
29. van Leeuwen, F. X., den Tonkelaar, E. M., and van Logten, M. J. (1983) Toxicity of sodium bromide in rats: effects on endocrine system and reproduction, *Food Chem. Toxicol. 21*, 383−389.
30. Nielsen, F. H. (1996) Other Trace Elements, in *Present Knowledge in Nutrition* (Ziegler, E. E., and Filer, L. L. Jr., Eds.) 7th ed., pp 353−377, ILSI Press: Washington, DC.
31. Alumot, E., Nachtomi, E., Kempenich-Pinto, O., Mandel, E., and Schindler, H. (1968) The effect of ethylene dibromide in feed on the growth, sexual development and fertility of chickens, *Poult. Sci. 47*, 1979−1985.
32. Pavelka, S. (2004) Metabolism of bromide and its interference with the metabolism of iodine, *Physiol. Res. 53 Suppl. 1*, S81−S90.
33. Buchberger, W., Holler, W., and Winsauer, K. (1990) Effects of sodium bromide on the biosynthesis of thyroid hormones and brominated/iodinated thyronines, *J. Trace Elem. Electrolytes Health Dis. 4*, 25−30.
34. Wu, W., Chen, Y., d' Avignon, A., and Hazen. S. L. (1999) 3-Bromotyrosine and 3,5-dibromotyrosine are major products of protein oxidation by eosinophil peroxidase: potential markers for eosinophil-dependent tissue injury in vivo, *Biochemistry 38*, 3538−3548.
35. Wu, W., Samoszuk, M. K., Comhair, S. A., Thomassen, M. J., Farver, C. F., Dweik, R. A., Kavuru, M. S., Erzurum, S. C., Hazen, S. L. (2000) Eosinophils generate brominating oxidants in allergen-induced asthma, *J. Clin. Invest. 105*, 1455−1463.
36. MacPherson, J. C., Comhair, S. A., Erzurum, S. C., Klein, D. F., Lipscomb, M. F., Kavuru, M. S., Samoszuk, M. K., and Hazen, S. L. (2001) Eosinophils are a major source of nitric oxide-derived oxidants in severe asthma: characterization of pathways available to eosinophils for generating reactive nitrogen species, *J. Immunol. 166*, 5763−5772.
37. Henderson, J. P., Byun, J., Williams, M. V., McCormick, M. L., Parks, W. C., Ridnour, L. A., and Heinecke, J. W. (2001) Bromination of deoxycytidine by eosinophil peroxidase: a mechanism for mutagenesis by oxidative damage of nucleotide precursors, *Proc. Natl. Acad. Sci. U.S.A. 98*, 1631−1636.
38. Stuehr, D. J. (1999) Mammalian nitric oxide synthases, *Biochim. Biophys. Acta 1411*, 217−230.
39. Nathan, C., and Xie, Q. W. (1994) Nitric oxide synthases: roles, tolls, and controls, *Cell 78*, 915−918.
40. Abu-Soud, H. M., Ichimori, K., Nakazawa, H., and Stuehr, D. J. (2001) Regulation of inducible nitric oxide synthase by self-generated NO, *Biochemistry 40*, 6876−6881.
41. Hurshman, A. R., and Marletta, M. A. (1995) Nitric oxide complexes of inducible nitric oxide synthase: spectral characterization and effect on catalytic activity, *Biochemistry 34*, 5627−5634.
42. Mitra, S. N., Slungaard, A., and Hazen, S. L. (2000) Role of eosinophil peroxidase in the origins of protein oxidation in asthma, *Redox. Rep. 5*, 215−224.
43. Thayer, J. R., and Huffaker, R. C. (1980) Determination of nitrate and nitrite by high-pressure liquid chromatography: comparison with other methods for nitrate determination, *Anal. Biochem. 102*, 110−119.
44. Jorg, A., Pasquier, J. M., and Kelebanoff, S. J. (1982) Purification of horse eosinophil peroxidase, *Biochim. Biophys. Acta 701*, 185−191.
45. van Dalen, C. J., Whitehouse, M. W., Winterbourn, C. C., and Kettle, A. J. (1997) Thiocyanate and chloride as competing substrates for myeloperoxidase, *Biochem. J. 327*, 487−492.
46. Bolscher, B. G., Plat, H., and Wever, R. (1984) Some properties of human eosinophil peroxidase, a comparison with other peroxidases, *Biochim. Biophys. Acta 784*, 177−186.
47. Carlson, M. G., Peterson, C. G., and Venge, P. (1985) Human eosinophil peroxidase: purification and characterization, *J. Immunol. 134*, 1875−1879.
48. Furtmuller, P. G., Burner, U., Regelsberger, G., Obinger, C. (2000) Spectral and kinetic studies on the formation of eosinophil peroxidase compound I and its reaction with halides and thiocyanate, *Biochemistry 39*, 15578−15584.
49. Furtmuller, P. G., Jantschko, W., Regelsberger, G., and Obinger, C. (2001) Spectral and kinetic studies on eosinophil peroxidase compounds I and II and their reaction with ascorbate and tyrosine, *Biochim. Biophys. Acta 1548*, 121−128.
50. Abu-Soud, H. M., and Hazen, S. L. (2001) Interrogation of heme pocket environment of mammalian peroxidases with diatomic ligands, *Biochemistry 40*, 10747−10755.
51. Furtmuller, P. G., Zederbauer, M., Jantschko, W., Helm, J., Bogner, M., Jakopitsch, C., and Obinger, C. (2005) Active site structure and catalytic mechanisms of human peroxidases, *Arch. Biochem. Biophys. 445*, 199−213.

52. Kettle, A. J., and Winterbourn, C. C. (2001) A kinetic analysis of the catalase activity of myeloperoxidase, *Biochemistry 40*, 10204−10212.
53. Andreadis, A. A., Hazen, S. L., Comhair, S. A., and Erzurum, S. C. (2003) Oxidative and nitrosative events in asthma, *Free Radic. Biol. Med. 35*, 213−225.
54. Brennan, M. -. L., Wu, W., Fu, X., Shen, Z., Song, W., Frost, H., Vadseth, C., Narine. L., Lenkiewicz, E., Borchers, M. T., Lusis, A. J., Lee, J. J., Lee, N. A., Abu-Soud, H. M., Ischiropoulos, H., and Hazen, S. L. (2002) A tale of two controversies. Defining both the role of peroxidases in nitrotyrosine formation in vivo using eosinophil peroxidase and myeloperoxidase-deficient mice, and the nature of peroxidase-generated reactive nitrogen species, *J. Biol. Chem. 277*, 17415−17427.
55. van der Vliet, A., Eiserich, J. P., and Cross, C. E. (2000) Nitric oxide: a pro-inflammatory mediator in lung disease? *Respir. Res. 1*, 67−72.
56. Xu, W., Zheng, S., Dweik, R. A. and Erzurum, S. C. (2006) The role of epithelial NO in airway viral infection, *Free Radic. Biol. Med. 41*, 19−28.
57. Tahboub, Y. R., Galijasevic, S., Diamond, M. P., and Abu-Soud, H. M. (2005) Thiocyanate modulates the catalytic activity of mammalian peroxidases, *J. Biol. Chem. 280*, 26129−26136.
58. Zeng, J., and Fenna, R. E. (1992) X-ray crystal structure of canine myeloperoxidase at 3 A resolution, *J. Mol. Biol. 226*, 185−207.
59. Davey, C. A., and Fenna, R. E. (1996) 2.3 A resolution X-ray crystal structure of the bisubstrate analogue inhibitor salicylhydroxamic acid bound to human myeloperoxidase: a model for a prereaction complex with hydrogen peroxide, *Biochemistry 35*, 10967−1097.
60. Fiedler, T. J., Davey, C. A., and Fenna, R. E. (2000) X-ray crystal structure and characterization of halide-binding sites of human myeloperoxidase at 1.8 Å resolution, *J. Biol. Chem. 275*, 11964−11971.
61. Bakkenist, A. R. J., De B.oer, J. E. G., Plat, H., and Wever, R. (1980) The halide complexes of myeloperoxidase and the mechanism of the halogenation reactions, *Biochim. Biophys. Acta 613*, 337−348.
62. van der Vliet, A., Eiserich, J. P., Halliwell, B., and Cross, C. E. (1997) Formation of reactive nitrogen species during peroxidase-catalyzed oxidation of nitrite. A potential additional mechanism of nitric oxide-dependent toxicity, *J. Biol. Chem. 272*, 7617−7625.
63. van Dalen, C. J., Winterbourn, C. C., and Kettle, A. J. (2006) Mechanism of nitrite oxidation by eosinophil peroxidase: implications for oxidant production and nitration by eosinophils, *Biochem. J. 394*, 707−713.
64. Proteasa, G., Tahboub, Y. R., Galijasevic, S., Raushel, F. M., and Abu-Soud, H. M. (2006) Kinetic evidence supports the existence of two halide-binding sites that display distinct impact on the heme iron microenvironment in myeloperoxidase, *Biochemistry*, in press.
65. Andrews, P. C., and Krinsky, N. I. (1982) A kinetic analysis of the interaction of human myeloperoxidase with hydrogen peroxide, chloride ions, and protons, *J. Biol. Chem. 257*, 13240−13245.
66. Harrison, J. E., and Schultz, J. (1976) Studies on the chlorinating activity of myeloperoxidase, *J. Biol. Chem. 251*, 1371−1374.
67. Wever, R., Kast, W. M., Kasinoedin, J. H., and Boelens, R. (1982) The peroxidation of thiocyanate catalysed by myeloperoxidase and lactoperoxidase, *Biochim. Biophys. Acta 709*, 212−219.
68. Singh, A. K., Singh, N., Bhushan, A., Singh, T. P. Structure of Bovine Lactoperoxidase at 2.3 Å resolution, in press.
69. De Gioia, L., Ghibaudi, E. M., Laurenti, E., Salmona, M., and Ferrari, R. P. (1996) A theoretical three-dimensional model for lactoperoxidase and eosinophil peroxidase, built on the scaffold of the myeloperoxidase X-ray structure, *J. Biol. Inorg. Chem. 1*, 476−485.
70. Kunishima, N., Fukuyama, K., Matsubara, H., Hatanaka, H., Shibano, Y., and Amachi, T. (1994) Crystal structure of the fungal peroxidase from Arthromyces ramosus at 1.9 Å resolution. Structural comparisons with the lignin and cytochrome c peroxidases, *J. Mol. Biol. 235*, 331−344.
71. Patterson, W. R., and Poulos, T. L. (1995) Crystal structure of recombinant pea cytosolic ascorbate peroxidase, *Biochemistry 34*, 4331−4341.
72. Schuller, D. J., Ban, N., Huystee, R. B., McPherson, A., and Poulos, T. L. (1996) The crystal structure of peanut peroxidase, *Structure 4*, 311−321.
73. Bosshard, H. R., Anni, H., and Yonetani, T. (1991) *Peroxidases in Chemistry and Biology*, Vol. II, pp 51−84, CRC Press, Boca Raton, FL.
74. Finzel, B. C., Poulos, T. L., and Kraut, J. (1984) Crystal structure of yeast cytochrome c peroxidase refined at 1.7-A resolution, *J. Biol. Chem. 259*, 13027−13036.
75. Gajhede, M., Schuller, D. J., Henriksen, A., Smith, A. T., and Poulos, T. L. (1997) Crystal structure of horseradish peroxidase C at 2.15 Å resolution, *Nat. Struct. Biol. 4*, 1032−1038.
76. Mozzarelli, A., and Rossi, G. L. (1996) Protein function in the crystal, *Annu. Rev. Biophys. Biomol. Struct. 25*, 343−365.
77. Barrick, D. (1995) Depletion and replacement of protein metal ligands, *Curr. Opin. Biotechnol. 6*, 411−418.
78. Cooper, C. E. (1999) Nitric oxide and iron proteins, *Biochim. Biophys. Acta 1411*, 290−309.
79. Abu-Soud, H. M., Wu, C., Ghosh, D. K., and Stuehr, D. J. (1998) Stopped-flow analysis of CO and NO binding to inducible nitric oxide synthase, *Biochemistry 37*, 3777−37786.
80. Uetani, K., Der, S. D., Zamanian-Daryoush, M., de La Motteqq, C., Lieberman, B. Y., Williams, B. R., and Erzurum, S. C. (2000) Central role of double-stranded RNA-activated protein kinase in microbial induction of nitric oxide synthase, *J. Immunol. 165*, 988−996.
81. Zheng, S., De, B. P., Choudhary, S., Comhair, S. A., Goggans, T., Slee, R., Williams, B. R., Pilewski, J., Haque, S. J., and Erzurum, S. C. (2003) Impaired innate host defense causes susceptibility to respiratory virus infections in cystic fibrosis, *Immunity 18*, 619−630.
82. Guo, F. H., Comhair, S. A., Zheng, S., Dweik, R. A., Eissa, N. T., Thomassen, M. J., Calhoun, W., and Erzurum, S. C. (2000) Molecular mechanisms of increased nitric oxide (NO) in asthma: evidence for transcriptional and post-translational regulation of NO synthesis, *J. Immunol. 164*, 5970−5980.
83. Dweik, R. A., Comhair, S. A., Gaston, B., Thunnissen, F. B., Farver, C., Thomassen, M. J., Kavuru, M., Hammel, J., Abu-Soud, H. M., and Erzurum, S. C. (2001) NO chemical events in the human airway during the immediate and late antigen-induced asthmatic response, *Proc. Natl. Acad. Sci. U.S.A. 98*, 2622−2627.

BI061177U